Original Article

Experimental Assessment of Proton Dose Calculation Accuracy in Small-Field Delivery Using a Mevion S250 Proton Therapy System

Kyle D. DePew, Salahuddin Ahmad, Hosang Jin

Department of Radiation Oncology, University of Oklahoma Health Sciences Centre, Oklahoma City, Oklahoma, USA

Abstract

Purpose: Dose calculation accuracy of the Varian Eclipse treatment planning system (TPS) is empirically assessed for small-aperture fields using a Mevion S250 double scattering proton therapy system. **Materials and Methods:** Five spherical pseudotumors were modeled in a RANDO head phantom. Plans were generated for the targets with apertures of 1, 2, 3, 4, or 5 cm diameter using one, two, and three beams. Depth-dose curves and lateral profiles of the beams were taken with the planned blocks and compared to Eclipse calculations. Dose distributions measured with EBT3 films in the phantom were also compared to Eclipse calculations. Film quenching effect was simulated and considered. **Results:** Depth-dose scans in water showed a range pullback (up to 2.0 mm), modulation widening (up to 9.5 mm), and dose escalation in proximal end and sub-peak region (up to 15.5%) when compared to the Eclipse calculations for small fields. Measured full width at half maximum and penumbrae for lateral profiles differed <1.0 mm from calculations for most comparisons. In the phantom study, Eclipse TPS underestimated sub-peak dose. Gamma passing rates improved with each beam added to the plans. Greater range pullback and modulation degradation versus water scans were observed due to film quenching, which became more noticeable as target size increased. **Conclusions:** Eclipse TPS generates acceptable target coverage for small targets with carefully arranged multiple beams despite relatively large dose discrepancy for each beam. Surface doses higher than Eclipse calculations can be mitigated with multiple beams. When using EBT3 film, the quenching effect should be considered.

Keywords: Pencil-beam algorithm, proton therapy, small-field dosimetry

Received on: 15-03-2018 **Review completed on: 18-10-2018** **Accepted on: 19-10-2018**

Introduction

Proton therapy is a useful modality for clinical targets situated near vital structures due to its sharp distal dose fall-off beyond the target and lower entrance dose relative to the intended target. This offers advantages over photon treatments, which also deposit dose on the distal side of the target. Variable modulation of the spread-out Bragg peak (SOBP) of proton beams permits a flat dose distribution through a tumor's thickness that cannot be accomplished without utilizing multiple photon fields involving more healthy tissue.

Previous works have summarized small-field effects in photon therapy,[1,2] electron therapy,[3] and proton therapy.[4,5] While proton therapy has obvious advantages, small fields present difficulties because fluence distributions are not easily modeled and extra precautions in dosimetry must be taken. The study of small-field dosimetry is similarly crucial for proton stereotactic radiosurgery, when the target is small and the field is smaller than 4.5 cm in diameter.[6] The primary mechanisms which affect depth-dose distributions in proton therapy are multiple Coulomb scattering, nuclear interactions, and a varying stopping power relationship. Dosimetric impact of scattered dose from aperture edge increases as field size decreases,[7] so dose calculation is less straightforward. A variable fluence will also complicate calculation for these interactions.

A method for determining output factors in small proton fields using a Monte Carlo (MC) code has been presented by

Address for correspondence: Dr. Hosang Jin,
800 Ne 10th St, L100, Oklahoma City, Ok 73104, USA.
E-mail: hosang-jin@ouhsc.edu

Access this article online

Quick Response Code:

Website: www.jmp.org.in

DOI: 10.4103/jmp.JMP_33_18

How to cite this article: DePew KD, Ahmad S, Jin H. Experimental assessment of proton dose calculation accuracy in small-field delivery using a mevion S250 proton therapy system. J Med Phys 2018;43:221-9.

Fontenot *et al*.[4] This study found that the use of compensators worsened agreement between measurements and models. In high-dose gradient regions, differences between actual and calibration output (D/monitor unit [MU]) values exceeded 20% with compensator but fell below 10% without compensator. Bednarz *et al*.[5] reported that a pencil beam algorithm had dosimetric limitations in predicting hot and cold spots and range degradation in treating small volumes. They found that the overall dose differences between their in-house calculation and MC calculation were within 3% for small field proton treatments. Daartz *et al*.[6] investigated the effects of small field sizes in proton treatment and found that the output factor was range and modulation width-dependent. For example, for a range of 22.4 cm, a 2 cm aperture reduced output by 23.7% compared to an open field, while the 4 cm aperture only reduced this output by 4.1%. However, the output only varied by <3% when fields whose modulation differed by 16.8 cm were compared. They also found that air gap was a significant factor on their results. Magro *et al*.[8] investigated the performance of the Siemens *syngo* treatment planning system (TPS) versus the FLUKA MC model for a scanning proton treatment system and cautioned against using the TPS for small fields and shallow targets where the ratio of the field size to the modeled pencil-beam full width at half maximum (FWHM) was <2. They also concluded that the pencil beam's single Gaussian approximation is inadequate to predict lateral spreading after a range shifter for shallow targets of dimensions smaller than 3 cm.

During the commissioning of the S250 double-scattering proton therapy system (Mevion Medical Systems, Littleton, MA, USA), depth-dose profiles of small (≤5 cm diameter) fields in water showed relatively larger dosimetric errors compared to TPS calculations especially in the sub-peak and entrance regions. The purpose of this study is to empirically determine the accuracy of the Varian Eclipse (Palo Alto, CA; version 11) calculation algorithm for small fields for the S250 proton therapy unit in patient geometry. In this work, depth-dose profiles are measured using Gafchromic EBT3 film inserted into an anthropomorphic head phantom for small centrally situated pseudobrain tumors and compared to corresponding TPS calculations. When the Gafchromic film is parallel to the proton beam, a relatively higher under-response in the Bragg peak region occurs due to higher linear energy transfer (LET) of low-energy protons. This quenching effect may be attributed to a higher density of free radicals produced toward the distal portion of the proton beam, resulting in significant recombination and fewer polymerization events.[9] The quenching effect is simulated and considered for analysis of film measurements. In addition, the small field proton beams used for the treatment plans are characterized by comparing depth-dose curves in water and lateral profiles to those of the Eclipse calculations.

Materials and Methods

Proton delivery system

Investigations were performed using the Mevion S250 compact double-scattering proton therapy system. The Mevion S250 possesses 24 options consisting of 12 large, 5 deep, and 7 small options. An "option" refers to a range group determined by a specific combination of beam modifying devices (scatterers, modulation wheels, and range shifters). Mevion defines the range (R) as the depth of the distal 90% dose point and the modulation (M) as the width between the distal 90% and proximal 95% dose points, normalized at the middle of the SOBP. The large options vary in range from 5.0 to 25.0 g/cm^2 with a large applicator (nominal diameter of 25 cm). The deep options have ranges between 20.1 and 32.0 g/cm^2 with a small applicator (nominal diameter of 14 cm), and the small options have ranges between 5.0 and 20.0 g/cm^2 with the small applicator. The minimum modulation is 2.0 g/cm^2, and the maximum is equal to the range selected for the small options and most of the large options (excepting options 1–3: 20.0 g/cm^2) and 10.0 g/cm^2 for all deep options. The option selected corresponds to a unique combination of field size and range using 7 first scatterers, 14 modulation wheels, 3 second scatterers, 2 final absorber wheels, and the final absorber plates. Detailed descriptions of the system and the commissioning process of the planning system can be found in previous publications.[10-12]

Eclipse calculation algorithm

The calculation algorithm of the Varian Eclipse TPS modeled each individual energy that made up the SOBP.[13] These individual energies were referred to as "energy layers." Within each energy layer, the field was split into a series of beamlets which were perpendicular to the surface plane of the medium and whose energy spectrum was taken to be Gaussian about the nominal energy of the beamlet. The dose was calculated in three steps. First, basic physical parameters of the beamlet were calculated such as the depth-dose curve and scattering behavior in water. Ranges listed in ICRU Report 49[14] were taken to be ranges in the continuous slowing down approximation, which were then used to calculate stopping power for primary protons, secondary protons, and recoil particles in a divergent beam grid. The second step involved undisturbed proton fluence calculation in air, based on scattering behavior and the inverse square law. Finally, dose calculation in the patient was derived from the proton fluence convolved with the beamlet dose, taking into account primary protons, secondary protons, and recoil particles, in their interactions with the patient's composition as seen in computed tomography (CT) images. The resulting dose calculations for all energy layers were then summed together within each voxel to obtain the final dose distribution.

Treatment planning and output calibration

To investigate dosimetric accuracy of small beams in proton beam delivery, the head of an Alderson RANDO phantom (Radiology Support Devices, Long Beach, CA, USA) was scanned on a Base of Skull (BoS) frame (QFix, Avondale, PA) in a Discovery CT scanner (GE Healthcare, Little Chalfont, United Kingdom) with slice thickness of 1.3 mm and pixel resolution of 0.51 mm. Five spherical pseudo targets (clinical target volume [CTV] diameters of 0.5, 1, 2, 3, and

4 cm) were contoured at the center of the brain, equidistant from each ear and the occiput in the Varian Eclipse TPS. Five different aperture sizes of 1, 2, 3, 4 and 5 cm diameter were employed for CTV diameters of 0.5, 1, 2, 3, and 4 cm, respectively. Air gaps were marginally adjusted to allow the same physical aperture size for all three beams in each plan. The five apertures were fabricated by pouring Cerrobend™ around three-dimensional-printed plastic cylinders of the necessary diameter in a reusable external stainless steel ring[15] for the 14 cm applicator.

Each plan was designed to deliver one of 28 fractions (a fractional dose of 180 cGy) to the CTV delivering a cumulative dose of 5040 cGy. The plans were normalized such that the 100% prescribed isodose line covered 99% of the CTV. The distal margin was calculated as 3.5% × R + 0.15 g/cm^2. Options 21 and 22 (small options) were used to obtain the planned ranges and modulation widths listed in Table 1. Three treatment plans were created using one, two, and three beams for each target size to investigate dependence of the target coverage and dose to normal tissues on the number of beams. The one-beam plans consisted of a left lateral field only. The two-beam plans added a right lateral field to the one-beam plans, and the three-beam plans added an occipital field whose path was perpendicular to the two-beam combination. All beams were coplanar to a transverse plane to facilitate dose measurement by film inserted into the phantom.

The Eclipse TPS did not provide MUs for the double scattering proton system. Outputs (cGy/MU) for all of the beams were calibrated at the isocenter set at mid-SOBP depth (R-M/2) with the corresponding apertures and planned air gaps following the International Atomic Energy Agency TRS-398 protocol.[16] To minimize dosimetric uncertainty during small aperture measurements, range compensators were not used in this study. An Exradin A16 (collecting volume = 0.007 cc; Standard Imaging Inc., Middleton, WI) ionization chamber (IC) was used for output measurements after cross-calibration with an Exradin A12 IC in an MP1 water tank (PTW, Freiburg, Germany) using a reference field (option 20, R = 15.0 g/cm^2, M = 10.0 g/cm^2, and field size = 10 cm × 10 cm).

Table 1: Ranges and modulations of treatment plans

Aperture diameter (CTV diameter)	Beam orientation	Range (g/cm^2) (proton energy)	Modulation (g/cm^2)
1 cm (0.5 cm)	LT LAT	9.1 (110 MeV)	2.2
	RT LAT	9.6 (113 MeV)	2.4
	PA	10.7 (121 MeV)	2.1
2 cm (1.0 cm)	LT LAT	9.4 (112 MeV)	2.8
	RT LAT	10.9 (122 MeV)	4.2
	PA	10.7 (121 MeV)	2.3
3 cm (2.0 cm)	LT LAT	10.0 (116 MeV)	4.0
	RT LAT	11.4 (125 MeV)	5.3
	PA	11.3 (124 MeV)	3.4
4 cm (3.0 cm)	LT LAT	11.2 (124 MeV)	5.7
	RT LAT	12.0 (129 MeV)	6.4
	PA	11.9 (128 MeV)	4.5
5 cm (4.0 cm)	LT LAT	12.0 (129 MeV)	7.0
	RT LAT	12.5 (132 MeV)	7.4
	PA	12.4 (131 MeV)	5.6

LT LAT: Left lateral, RT LAT: Right lateral, PA: Posterior-anterior, CTV: Clinical target volume

Depth-dose measurement

The accuracy of SOBP calculation in the Eclipse TPS was assessed by obtaining depth-dose curves for each beam with the aperture block and planned air gap. The depth-dose profile was scanned in the MP1 water tank with the isocenter set at mid-SOBP depth and then normalized to the mid-SOBP value. The Exradin A16 and PTW TN 31014 (collecting volume = 0.015 cc) ICs were used as field and reference chambers, respectively. The offset of the effective point of measurement from the central electrode for the small cylindrical field chamber was determined to be negligible (mean difference of ~ 0 mm especially at the distal 90% dose point) by comparing the depth-dose scan with a PTW Advanced Markus chamber for several selected beams. The normalized depth-dose curves were compared with those from Eclipse, calculated in a virtual water phantom. Range, modulation width, dose at depth of R-M, and dose at 0.5 g/cm^2 depth were compared. To examine the dependence of calculation accuracy on field size, the same 15 beams were also scanned with a 14 cm diameter field and compared with those from Eclipse calculations.

Lateral profile measurement

Lateral profiles for all of the 15 beams in Table 1 were measured by placing Gafchromic EBT3 (Ashland Advanced Materials, Bridgewater, NJ, USA) film under solid water at the corresponding mid-SOBP depth with the corresponding aperture block and planned air gap at a gantry angle of 0°. The films were scanned at least 24 h after exposure to allow for full development. Films were scanned at 96 dpi resolution in 48-bit TIFF file format using an Epson (Suwa, Japan) 10000XL scanner. For dose calibration, a series of 10 separate film pieces (4 cm × 5 cm each) were exposed to 0, 25, 50, 100, 150, 200, 250, 300, 350 and 400 cGy, respectively, using the reference field (R = 15 g/cm^2 and M = 10 g/cm^2; film at isocenter). The profile films were then calibrated using a third-order polynomial fit of optical density to dose and normalized to the dose at the center. Lateral profiles were extracted in X (inline) and Y (crossline) directions and compared to those from Eclipse calculations performed in the virtual water phantom using the same beam setup regarding field size (FWHM) and penumbra width (defined as the distance between 20% and 80% of the maximum profile value). All the films in this study were analyzed with the red channel only (16-bit depth) using an in-house MATLAB (Mathworks, Natick, MA, USA) program.

Dose comparison for the phantom study

Two-dimensional dose distribution for a beam was measured for each target using Gafchromic EBT3 film, which was cut to match the cross section of the phantom slice and inserted

into the RANDO head phantom. Three fiducial points (anterior, left, and right) were marked on the film to indicate laser alignment after setup verification to facilitate later image registration. The measured films were calibrated using the same fit as the lateral profile measurement and compared to the corresponding Eclipse dose maps. The dose maps were extracted at a resolution of 1 mm/pixel in DICOM format. A gamma analysis[17] was then performed using criteria of 2%/2 mm (dose difference in percent prescription/distance to agreement) and 3%/3 mm using an in-house MATLAB software program. To evaluate dose agreement at the surface and entrance regions of the SOBP, two different evaluation thresholds of 10% and 50% of the maximum calculation dose were applied. The threshold of 50% was intentionally selected to compare the target region only because the dosimetric uncertainty of the Eclipse calculation was much higher in the sub-peak and entrance regions.

In this proton system, SOBP was constructed as a weighted summation of modulated Bragg peaks. Weighting of each Bragg peak corresponded to an angular section of a step or sector in the range modulation wheel, as this determined the proportion of time when that particular step thickness was located in front of the proton beam. SOBP can be estimated using the sector angles, step thicknesses of the wheel, and gating information (beam stop angle for a specific modulation) provided by the vendor. Table 2 detailed the weighting for each of the three options used in this study. Film quenching was LET-dependent and was stronger toward the distal portion of the proton beam. Peucelle *et al*.[18] found that the film measurement value of the Bragg peak itself can be reduced by up to 30% with 100 MeV pristine Bragg peaks (7.7 cm water equivalent depth). The effect decreased with incident particle energy, as another study[19] found a quenching factor of 10% for 148.8 MeV protons. A preliminary measurement showed that the quenching factor of the Gafchromic EBT3 film was estimated to be about 11% for the energies used in this study. Figure 1 shows an example simulation of quenching effect for the 3 cm aperture right lateral beam implemented in an in-house MATLAB program. The simulated quenching measurement was normalized to the mid-SOBP point because the beam was calibrated at that point.

Results

Depth-dose comparison of planned beams

The depth-dose scans in water for the 2 cm posterior-anterior beam are shown in Figure 2. For this specific beam, three distinct effects were observed for the small field when compared to the large field (14 cm aperture): A slight pullback of range, an obvious increase in the proximal dose relative to the peak value, and degradation of the SOBP and distal falloff. For all 15 beams, the range difference (measurement - calculation) for small beams ranged from −2.0 mm (1 cm posterior-anterior and 4 cm right lateral) to 0.6 mm (3 cm left lateral), while the differences were within ± 0.6 mm for all of the large fields, as shown in Table 3. The average modulation differences were 3.4 mm (standard deviation [SD]: 2.6 mm) and 0.1 mm (SD: 1.6 mm) for small and large fields, respectively. Due to the increase in the proximal dose, the modulation width was found to be wider for small fields. The average dose differences at depth of *R*-*M* were 2.2% (SD: 1.9%) and 0.1% (SD: 1.6%) for small and large fields, respectively. The

Table 2: Bragg peak weighting for modulated beams selected from treatment plans

Option	Modulation width (g/cm²)	Peak-to-peak distance (g/cm²)	Bragg peak weighting (distal to proximal)
22	2.2	1.03	65.0%, 23.1%, 11.9% (3 peaks)
	2.8	1.03	58.9%, 20.9%, 14.9%, 5.3% (4 peaks)
	4.2	1.03	52.7%, 18.7%, 13.4%, 10.2%, 5.1% (5 peaks)
21	3.4	1.07	57.5%, 20.3%, 14.4%, 7.9% (4 peaks)
	5.3	1.07	50.1%, 17.7%, 12.5%, 9.5%, 7.5%, 2.7% (6 peaks)
	7.4	1.07	45.5%, 16.1%, 11.4%, 8.6%, 6.8%, 5.6%, 4.7%, 1.2% (8 peaks)
20	10.0	1.08	43.1%, 15.1%, 10.6%, 8.0%, 6.3%, 5.2%, 4.3%, 3.6%, 3.0%, 0.9% (10 peaks; film calibration)

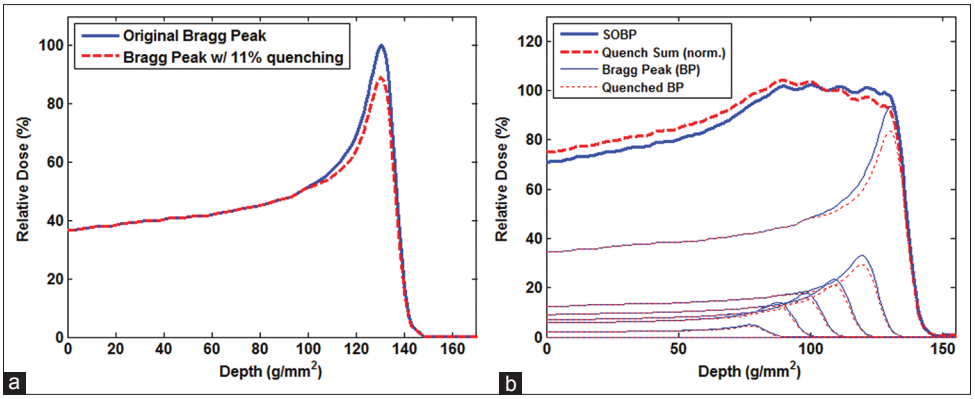

Figure 1: Quenching simulation for the right lateral beam of 3 cm aperture with a quenching factor of 11%. (a) Quenching simulation of a pristine Bragg peak and (b) quenching simulation of spread-out Bragg peak normalized to the middle of modulation

measured dose in the entrance region was also higher for small fields. The average dose differences at depth of 0.5 g/cm^2 were 10.6% (SD: 4.9%) and 0.2% (SD: 0.9%) for small and large fields, respectively.

Lateral profiles of planned beams

The measured lateral profiles agreed well with the corresponding calculations as shown in Figure 3. The differences in FWHM of the lateral profiles were within 1.2 mm of difference for all of the beams as summarized in Table 4. The mean FWHM differences for all 15 beams were −0.2 (SD: 0.5) mm in the lateral (X) direction and −0.5 (SD: 0.4) mm in the longitudinal (Y) direction with the couch angle of 0°. In all of these cases, the mean differences in penumbra size were negative, indicating that the Eclipse calculations predicted a slightly gentler slope on each side than was actually measured in the films.

Dose comparison for the phantom study

For accurate analysis of the EBT3 film measurement, quenching corrections should be properly considered in the Bragg peak regions. The quenching simulations of all the left lateral beams of the phantom study are shown in Figure 4. Owing to quenching-induced SOBP degradation, the SOBP became wider with increased target size when compared to the large-beam ion chamber (IC) scan in water [top row of Figure 4]. A similar SOBP degradation was seen in phantom head film measurements when compared to the Eclipse calculations [bottom row of Figure 4].

As predicted from depth-dose water scans, the measured dose was higher than the Eclipse calculation in low-dose entrance and sub-peak regions. However, the dose increase was higher than predicted by water scans, as seen in Figure 4 (bottom row). In general, normalizing the quenching

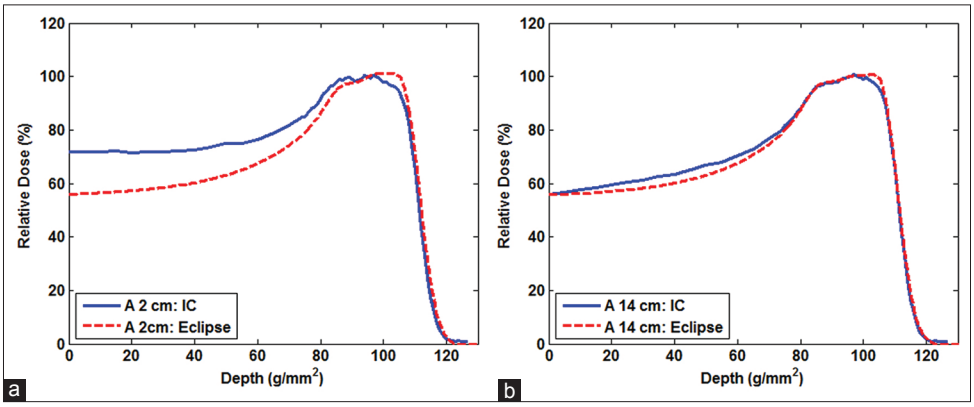

Figure 2: Comparison of the measured depth-dose profile to Eclipse calculations for the 2 cm posterior-anterior beam. Comparison of (a) 2 cm aperture beam to Eclipse calculations and (b) the large aperture (14 cm diameter) measurement to the Eclipse calculation

Table 3: Mean differences (measured - Eclipse) for the same ranges and modulations Standard deviations in parentheses

Aperture diameter (cm)	Range (mm)		Modulation (mm)		Dose at range - modulation (%)		Dose at 5 mm depth (%)	
	Small	Large (14 cm)	Small	Large (14 cm)	Small	Large (14 cm)	Small	Large (14 cm)
1	−0.6 (1.3)	−0.1 (0.2)	0.9 (2.0)	−1.2 (0.9)	0.9 (3.5)	−1.5 (1.9)	11.7 (9.9)	0.7 (0.4)
2	−0.9 (0.5)	0.0 (0.4)	2.9 (1.5)	−0.2 (0.8)	3.2 (1.0)	−0.1 (1.3)	13.8 (2.8)	0.7 (0.3)
3	0.3 (0.3)	−0.4 (0.1)	2.9 (1.5)	1.8 (1.5)	1.6 (1.1)	1.7 (0.5)	7.7 (0.5)	0.7 (0.4)
4	−0.6 (1.3)	−0.3 (1.2)	6.0 (3.3)	1.0 (1.9)	3.3 (1.7)	0.8 (1.6)	12.4 (3.7)	0.1 (0.3)
5	0.0 (0.4)	−0.3 (0.2)	4.3 (2.4)	−0.8 (1.2)	1.9 (1.1)	−0.4 (0.9)	7.7 (0.4)	−1.3 (0.9)

Table 4: Mean difference (measurement - Eclipse) for lateral profile parameters standard deviation in parentheses

Aperture diameter (cm)	X direction (lateral with couch=0°)			Y direction (longitudinal with couch=0°)		
	FWHM (mm)	Left penumbra (mm)	Right penumbra (mm)	FWHM (mm)	Superior penumbra (mm)	Inferior penumbra (mm)
1	−0.9 (0.1)	−0.8 (0.1)	−0.7 (0.0)	−0.7 (0.1)	−0.6 (0.0)	−0.7 (0.0)
2	−0.6 (0.1)	−0.8 (0.2)	−0.9 (0.3)	−1.1 (0.1)	−0.8 (0.1)	−0.9 (0.1)
3	−0.2 (0.3)	−1.0 (0.0)	−1.2 (0.1)	−0.5 (0.1)	−1.0 (0.1)	−1.1 (0.0)
4	0.1 (0.1)	−1.0 (0.1)	−1.0 (0.0)	−0.8 (0.2)	−0.7 (0.1)	−0.7 (0.1)
5	0.4 (0.1)	−1.0 (0.1)	−0.9 (0.0)	−0.5 (0.0)	−0.9 (0.1)	−1.0 (0.1)

FWHM: Full width at half maximum

simulation curves at the mid-SOBP yields increased surface dose measurements by 5% when compared to large-beam water scans [top row of Figure 4].

Dose comparisons for the phantom study are shown in Figure 5a-c. As predicted in the depth-dose scans, the measured doses were higher than the Eclipse calculations in low-dose entrance and sub-peak regions. The dose differences in these regions [the third rows in Figure 5a-c] were less pronounced as the number of beams was increased because each beam equally contributed to the target dose. The discrepancies were in the range of 10%–13% of prescription (one-beam plans), 6%–8% (two-beam plans), and 4%–5% (three-beam plans). Interestingly enough, distinct cold spots were found on the distal end of beams in the one-beam plans [the third row in Figure 5a] which indicated the pullback of range. This was consistent with the pullback of range by the degradation of SOBP in Figure 2 and the quenching effect in Figure 4.

The gamma passing rates at 10% and 50% thresholds are presented in Table 5. In general, the pass rates at both the 10% and 50% threshold increased with the number of beams.

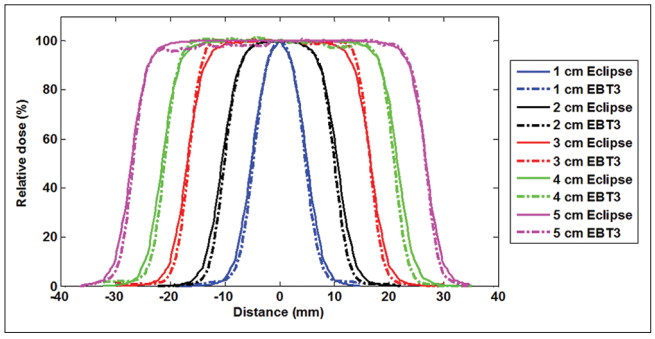

Figure 3: Comparison of lateral profiles (Y direction) taken for all of the left lateral beams. The full width at half maximums of the calculations is slightly wider than measurements. Measurements also show a slightly sharper penumbra

The gamma maps with 2%/2 mm in Figure 5 (the respective fourth rows) clearly show better agreement in the target regions (50% threshold) and more gamma test failures (γ >1) in the entrance and sub-peak regions.

Discussion

The Eclipse calculation algorithm predicted dose well for broad beam geometry; however, it produced relatively large dosimetric discrepancies for small fields as shown in Table 3. This may originate from inaccurate prediction of the fluence depletion[20] and slit scattering[21] for small beams. Protons are gradually removed through nuclear interactions from entrance to near the end of the beam range. As the field size is smaller, the fluence depletion of protons is more pronounced as a function of depth and substantially reduces the absorbed dose

Table 5: Gamma test results for different aperture sizes compared to Eclipse calculations

Number of beams	Aperture size (cm)	10% gamma threshold		50% gamma threshold	
		2%/2 mm	3%/3 mm	2%/2 mm	3%/3 mm
1	1	43.4	64.7	44.4	69.4
	2	35.7	52.7	27.4	42.8
	3	32.4	48.5	26.0	43.5
	4	35.7	55.5	33.0	54.1
	5	33.0	49.0	27.5	43.3
2	1	37.7	61.1	74.2	85.8
	2	35.2	52.5	79.0	90.8
	3	41.7	64.9	65.0	89.1
	4	39.5	54.6	65.4	85.8
	5	43.4	60.9	66.5	85.5
3	1	59.1	85.3	93.6	100.0
	2	42.4	61.1	93.9	100.0
	3	41.3	72.3	79.1	94.0
	4	67.8	82.2	79.9	93.6
	5	54.0	73.9	72.8	93.2

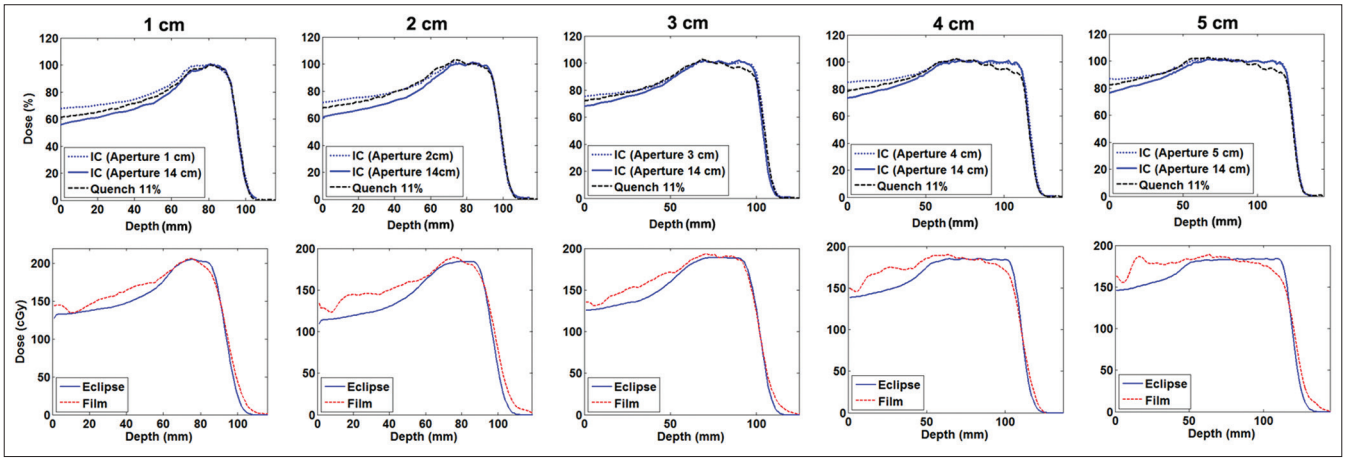

Figure 4: Quenching simulations and measurements of EBT3 film for the left lateral beams. Top row: Quenching simulations (normalized to the middle of modulation) and ionization chamber scans in water using small and large (14 cm; good agreement with Eclipse) beams. Bottom row: EBT3 film measurements and Eclipse calculations of the left lateral beams [profile scans of Figure 5a]

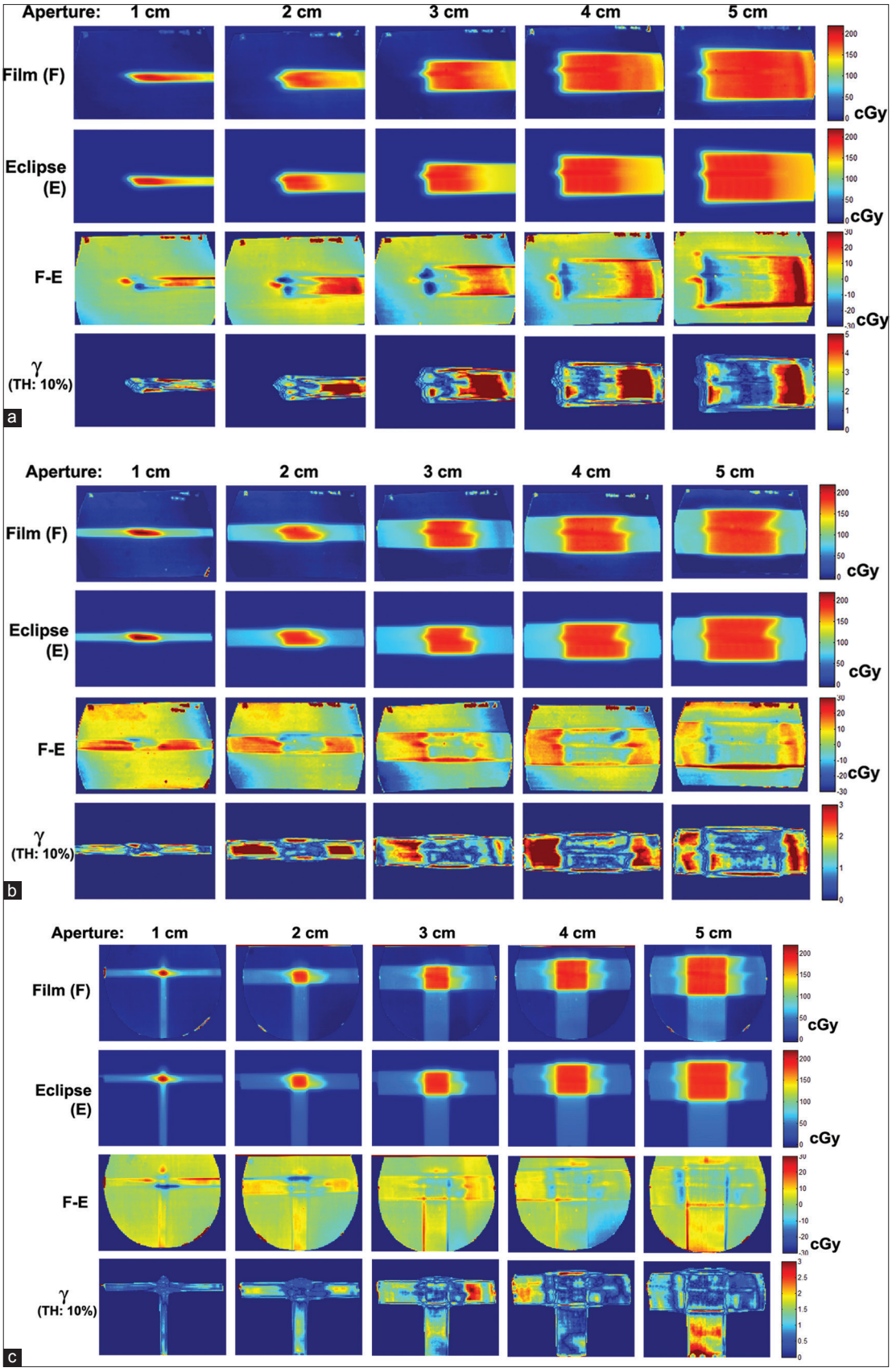

Figure 5: Dose comparisons for (a) one-beam, (b) two-beam, and (c) three-beam plans using different apertures. The third row displays the subtraction of the Eclipse calculation from the film measurement, while the bottom row displays the gamma test results, where colors indicate the value of the γ parameter

at the peak relative to the entrance dose. It appears that the actual fluence depletion of the proton therapy system is more dramatic than the Eclipse prediction. This results in a relative increase of sub-peak dose and slight widening of the SOBP which generally appears as a "slant" along the top of the SOBP with higher values shifted toward the proximal end [depth-dose scans with small apertures in the top row of Figure 4]. The relatively longer ranges calculated for the small fields as seen in Figure 2 might also be attributed to overestimation of the deepest Bragg peak (stemming from Eclipse's assumption of less fluence depletion) which usually has the highest peak and determines the range of the proton beam [Figure 1]. In addition, the Eclipse algorithm may underestimate the effect of slit scattering for small fields. Slit scattering occurs when protons strike the sides of the applicator aperture and lose energy in the process. The low-energy protons scattered back into the field from the edges increase surface and entrance dose. When the field size is small, the effect is more noticeable due to overlapping of slit-scattered protons at the field center. The slit scattering is also a function of air gap, and varying air gaps create different dosimetric discrepancies in the entrance regions of small beams.[21]

In this study, a general trend in the agreement between measurement and calculation regarding aperture size was not observed. This is because the different sets of R and M were used for different aperture sizes [Table 1]. In a separate water scan study,[22] noticeable degradations of SOBPs as a function of the modulation width for small fields were found. For $R = 15$ g/cm^2, the differences in modulation width and proximal dose were much larger for $M = 10$ g/cm^2 than $M = 2$ g/cm^2 using the small aperture blocks. This is because more Bragg peaks were used to generate a wider SOBP, in which the effect of fluence depletion has been more obvious.

The deficiencies of the small field beams can be mitigated by multiple-beam plans. Results of the phantom study showed that one-beam plans provided clinically unacceptable target coverage and substantially high sub-peak and entrance dose compared to treatment planning as shown in Figure 5a. Note that the surface dose increase in the phantom study is due to the accumulation of the small field effect and the normalization of film measurement. The degradations of the SOBPs and the dose reductions at the distal end of the beam in small fields [Figure 2] can theoretically be ameliorated by employing parallel opposed beams whose distal and proximal SOBP regions compensated for the dose uncertainty of the other. Carefully determined multiple beam angles offered the potential to compensate for degradation of the SOBP and to distribute the excess dose around the surface of the patient. The improvement in γ passing rate with increasing number of beams at the 50% threshold in Table 5 supports this proposed solution. In particular, the addition of the second beam to the first moved the γ passing rate above the 65.0% level in the target region (2%/2 mm) from 33% or lower in every case. Additional beams without an opposing partner also improved the result. It should be noted that each lateral beam compensated for high proximal dose with the range pullback in the other, which was mainly caused by film quenching. In reality, the range pullbacks and degradations of SOBPs were not as large as those film measurements based on the depth-dose scans in water as shown in Figure 4. It is expected that the target coverage and the γ passing rate without quenching would be better, especially for the larger targets. In addition, it was generally true that additional beams distributed the excess shallow dose such that dose uncertainty of individual entry was reduced by the number of beams. It is not practical to apply simple quenching correction factors based on water scans[18] in this study due to heterogeneity and various quenching factors for different modulation widths and energies. The integrated quenching effect can be disentangled from the Eclipse modeling accuracy for the small beams by cross comparison of the film measurements and the water scans with the corresponding Eclipse calculations.

The film measurement interestingly detected a cold region in the cranium for all aperture sizes as shown in Figure 4 (dose trough at a depth of ~1 g/cm^2). This result corresponds to an MC simulation for proton therapy using a slab head phantom by Jia *et al*.[23] This effect occurs because mass stopping power (in MeV cm^2/g) of bone is less than that of water or soft tissue for proton beams.[24] Considering the higher measured dose in small fields, it is obvious from the depth-dose profiles that the Eclipse calculation model does not accurately account for this effect in the cranium. This should, therefore, be taken into consideration when using the pencil beam algorithm for treatment planning.

Conclusions

Small aperture proton beams are problematic for the Eclipse pencil-beam calculation algorithm. The ranges for small aperture beams are generally shorter than Eclipse calculations. Modulations are wider (>~3 mm in water) for small apertures (1–5 cm diameter) in comparison to the Eclipse calculation. Doses at *R-M* and 0.5 g/cm^2 depth are increased relative to large (14 cm diameter) fields. The dose differences at 0.5 g/cm^2 depth in particular are much larger for the small apertures than for the large apertures. It is postulated that the Eclipse calculation algorithm underestimates the fluence depletion and slit scattering for small proton beams.

Dose increase proximal to the target should be evaluated to determine the acceptability of calculation, which may be improved by multiple beams. The Eclipse calculation algorithm also provides inaccurate dose calculation where the cranium is located for brain cases. However, the Eclipse calculation can provide clinically acceptable target coverage for small targets if the treatment plan is generated by multiple proton beams.

Quenching is crucial for any radiochromic film dosimetry when film is parallel to the beam. Quenching may not substantially affect small modulation beams (<5% dosimetric error for M <4 g/cm^2); however, it is of great importance to take the quenching effect into consideration for

larger targets. The quenching simulation method proposed in this study can play a useful role in understanding the quenching effect for SOBP measurement.

Financial support and sponsorship

Nil.

Conflicts of interest

There are no conflicts of interest.

References

1. Das IJ, Ding GX, Ahnesjö A. Small fields: Nonequilibrium radiation dosimetry. Med Phys 2008;35:206-15.
2. Alfonso R, Andreo P, Capote R, Huq MS, Kilby W, Kjäll P, *et al.* A new formalism for reference dosimetry of small and nonstandard fields. Med Phys 2008;35:5179-86.
3. Rustgi SN, Working KR. Dosimetry of small field electron beams. Med Dosim 1992;17:107-10.
4. Fontenot JD, Newhauser WD, Bloch C, White RA, Titt U, Starkschall G, *et al.* Determination of output factors for small proton therapy fields. Med Phys 2007;34:489-98.
5. Bednarz B, Daartz J, Paganetti H. Dosimetric accuracy of planning and delivering small proton therapy fields. Phys Med Biol 2010;55:7425-38.
6. Daartz J, Engelsman M, Paganetti H, Bussière MR. Field size dependence of the output factor in passively scattered proton therapy: Influence of range, modulation, air gap, and machine settings. Med Phys 2009;36:3205-10.
7. Titt U, Zheng Y, Vassiliev ON, Newhauser WD. Monte Carlo investigation of collimator scatter of proton-therapy beams produced using the passive scattering method. Phys Med Biol 2008;53:487-504.
8. Magro G, Molinelli S, Mairani A, Mirandola A, Panizza D, Russo S, *et al.* Dosimetric accuracy of a treatment planning system for actively scanned proton beams and small target volumes: Monte Carlo and experimental validation. Phys Med Biol 2015;60:6865-80.
9. Kirby D, Green S, Palmans H, Hugtenburg R, Wojnecki C, Parker D, *et al.* LET dependence of gafChromic films and an ion chamber in low-energy proton dosimetry. Phys Med Biol 2010;55:417-33.
10. Ferguson S, Ahmad S, Jin H. Implementation of output prediction models for a passively double-scattered proton therapy system. Med Phys 2016;43:6089.
11. Ferguson S, Chen Y, Ferreira C, Islam M, Keeling VP, Lau A, *et al.* Comparability of three output prediction models for a compact passively double-scattered proton therapy system. J Appl Clin Med Phys 2017;18:108-17.
12. Zhao T, Sun B, Grantham K, Rankine L, Cai B, Goddu SM, *et al.* Commissioning and initial experience with the first clinical gantry-mounted proton therapy system. J Appl Clin Med Phys 2016;17:24-40.
13. Varian Medical Systems. Proton Algorithm Reference Guide: Eclipse (Document ID: B504886R01, Revision A). Palo Alto, California, USA: Varian Medical Systems; 2013.
14. International Commission of Radiation Units. Report 49: Stopping Powers and Ranges for Protons and Alpha Particles. Bethesda, Maryland, USA: International Commission of Radiation Units and Measurements; 1993.
15. Chen H, Matysiak W, Flampouri S, Slopsema R, Li Z. Dosimetric evaluation of hybrid brass/stainless-steel apertures for proton therapy. Phys Med Biol 2014;59:5043-60.
16. International Atomic Energy Agency. Absorbed dose Determination in External Beam Radiotherapy: An International Code of Practice for Dosimetry Based on Standards of Absorbed dose to Water. Vienna, Austria: International Atomic Energy Agency; 2000.
17. Low DA, Harms WB, Mutic S, Purdy JA. A technique for the quantitative evaluation of dose distributions. Med Phys 1998;25:656-61.
18. Peucelle C, Nauraye C, Patriarca A, Hierso E, Fournier-Bidoz N, Martínez-Rovira I, *et al.* Proton minibeam radiation therapy: Experimental dosimetry evaluation. Med Phys 2015;42:7108-13.
19. Castriconi R, Ciocca M, Mirandola A, Sini C, Broggi S, Schwarz M, *et al.* Dose-response of EBT3 radiochromic films to proton and carbon ion clinical beams. Phys Med Biol 2017;62:377-93.
20. Newhauser WD, Zhang R. The physics of proton therapy. Phys Med Biol 2015;60:R155-209.
21. Hong L, Goitein M, Bucciolini M, Comiskey R, Gottschalk B, Rosenthal S, *et al.* A pencil beam algorithm for proton dose calculations. Phys Med Biol 1996;41:1305-30.
22. DePew KD, Jin H, Ahmad S. Accuracy of the Eclipse Pencil-Beam Algorithm in Small Fields for a Passively Scattered Proton Therapy System. Poster Presented at: AAPM 59th Annual Meeting. Denver, CO.; 2017.
23. Jia SB, Hadizadeh MH, Mowlavi AA, Loushab ME. Evaluation of energy deposition and secondary particle production in proton therapy of brain using a slab head phantom. Rep Pract Oncol Radiother 2014;19:376-84.
24. Singh H, Rathi SK, Verma AS. Stopping powers of protons in biological human body substances. Univ J Med Sci 2013;1:17-22.